# Large-scale side by side Stereo-PIV measurements in an automotive wind tunnel: Aerodynamic influence of ride height variations.

A. O. Erdogdu<sup>1,\*</sup>, S. Hüttig<sup>2</sup>, J. C. Londono Alfaro<sup>2</sup>, T. Gericke<sup>2</sup>, A. Schröder<sup>3,4</sup>

1: LaVision GmbH, Göttingen, Germany
2: Volkswagen AG, Wolfsburg, Germany
3: Institute of Aerodynamics and Flow Technology, German Aerospace Center (DLR), Göttingen, Germany
4: Institute of Transport Technology, Brandenburg University of Technology, Cottbus, Germany

\* Correspondent author: aerdogdu@lavision.de

Keywords: PIV Applications, Passenger Vehicle Aerodynamics, Large Scale PIV

#### **ABSTRACT**

In this investigation, we conducted large-scale Stereo PIV experiments in the flow around a Volkswagen ID.4. within the Aerodynamic and Aeroacoustic Wind Tunnel (AAK) at Volkswagen AG, Wolfsburg. The primary objective of these experiments was to investigate the effects of ride height variation on the near wake of the passenger vehicle using Stereo PIV, while minimizing wind tunnel occupancy. The measurements aimed to create datasets for CFD validation to improve virtual aerodynamic development capabilities of passenger vehicles. The experiment was performed on a 1:1 scale vehicle and multiple cross-sectional planes were scanned along the longitudinal axis of the vehicle. The impact of ride height alterations on the wake flow topology were evaluated. Average velocity vector fields were computed per case, providing comprehensive insights into the aerodynamic effects of diverse vehicle setups. A small change in the ride height has shown to have a significant impact on the wake topology. The results show that the electric SUV ID.4 can yield a wake topology similar to the estate back and fast/notchback type of vehicle, depending on the ride height. The normal ride height of the ID.4 shows to have a broader but lower wake region, with a significant downwash. The PIV results of this configuration show significant similarities to the wake topology of a fast back vehicle. Lowering the ride height by 15 mm has shown already to be enough to cause a global effect on the wake topology and to exhibit a narrower wake and recirculation region, like an estate back vehicle. Additionally, the association between the drag/lift coefficients and the wake topology of both configurations was discussed. Results have shown that sole measurements in the wake are not sufficient to fully explain changes in the determined drag or front lift coefficients. The rear lift coefficients however, indicate a stronger relationship with the near wake topology of the vehicle.

#### 1. Introduction

The significance of aerodynamics in the electric vehicle era has experienced a notable upsurge within the automotive industry over the past decade. A heightened emphasis has been placed on comprehending the flow dynamics around passenger vehicles (Petar Georgiev & Sorniotti, 2023).

While understanding the flow characteristics around a vehicle allows for a greater aerodynamic efficiency to be aimed and achieved, conducting exhaustive investigations on every vehicle model and configuration introduced to the market is impractical. Therefore, the automotive industry relies extensively on CFD results in conjunction with force balance measurements performed in the wind tunnel. The operational and maintenance costs associated with wind tunnels, combined with the required wind tunnel tests for every vehicle configuration, creates a vast time efficiency requirement in aerodynamic test facilities. Due to these reasons, as sophisticated and non-intrusive the Particle Image Velocimetry measurement technique in comparison to other velocity measurement techniques is, usually it is not the preferred solution in passenger car aerodynamic development. Developing a time and cost-efficient method of generating velocity measurement data with a high spatial resolution creates an opportunity to implement PIV more regularly in aerodynamic facilities of the automotive industry.

This experimental investigation aims to create a measurement concept capable of acquiring a large quantity of data in the shortest time via PIV. The objective was to rationalize the cost of wind tunnel operation by maximizing the variety, quality, and quantity of acquired data, while simultaneously exploring the impact of variations in vehicle configurations. A large-scale side-by-side PIV setup was developed to resolve the flow in cross-sectional measurement planes spanning the half symmetry of the ID.4. To ensure the rapid assembly for optimizing time efficiency, a relatively compact measurement setup was designed. Di-Ethyl-Hexyl-Sebacate (DEHS) particles were used as tracer particles, illuminated with 2x Quantel Evergreen 200 mJ/pulse lasers. The experiments were performed in the Aerodynamic and Aeroacoustic Wind Tunnel at Volkswagen AG (AAK).

The study also focuses on displaying the global aerodynamic effects of subtle changes in vehicle configurations. The impact of variations in the ride height on car wake aerodynamics was visualized through three-component (3C) velocity vector fields. Furthermore, the association between ride height changes, scale measurements, and differences in flow topology was discussed.

### 2. Experimental Setup

The experimental setup was constructed utilizing components from the X-95 rail and mounting system components. A construction containing the linear traversing system, cameras and both lasers was placed on a stable ground platform. The ground platform was used to establish a defined, leveled and static platform, on which the Stereo PIV equipment was attached. The need for a compact measurement system dictated the close proximity of cameras and lasers, requiring the cameras to be placed in a backward light scattering direction. This constraint, coupled with

limited light intensity and regulatory restrictions on seeding medium options (restricted to DEHS droplets), presented challenges in designing the experiment with optimal camera viewing angles. Figure 1 depicts the measurement setup in the wind tunnel. The setup contained two separate Stereo PIV systems, which were situated on two levels. The separate measurement planes were planned to be combined using a certain overlap between top and bottom laser light sheets and corresponding field of view. Figure 2 illustrates a sketch of the experimental setup with working distances in the wind tunnel during the planning phase, while the experimental apparatus employed during the measurements can be seen on Table 1. The planned field of view of the measurement can be seen on Figure 3. The control unit for both the traversing system and lasers, along with the measurement computer, was placed in the wind tunnel outside the shear layer. All devices, including the seeding device, were remotely controlled from the AAK control room.

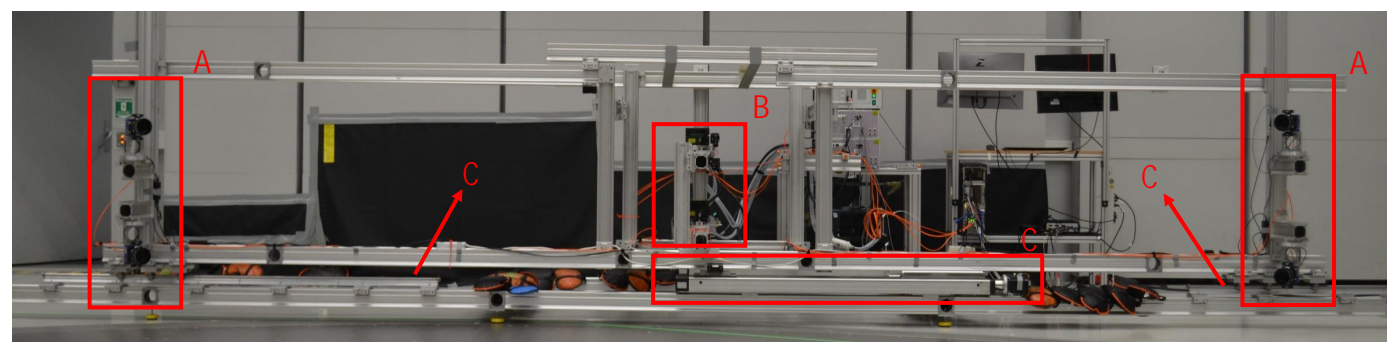


**Figure 1.** The measurement setup built in the test section, where A) indicates the location of the cameras, B) contains the laser configuration and C) displays the traversing system with rails.

Illumination of the measurement area of approximately 1700 x 1500 mm² was achieved using two Quantel Evergreen double-pulse lasers, each emitting 200 mJ per pulse. Two identical light sheet optics were created, containing a Galilean telescope for sheet thickness control and a cylindrical concave lens for light sheet expansion. Employing four scientific CMOS cameras with a resolution of 2560 x 2160 px from LaVision, a side-by-side stereo configuration in particle backward scattering direction was implemented on a motorized linear traversing system. The two stereo camera systems and the laser heads were placed on a two-level platform and two separate laser light sheets were generated. Translation of lasers and cameras was controlled through the DaVis software, facilitating a modular dynamic system designed to scan multiple planes in the vehicle's wake. The system enabled a fully automated traversing along 1500 mm in flow direction, supplemented by a stabilized rail system for manual adjustments, expanding the longitudinal access to the vehicle to approximately 3000 mm.

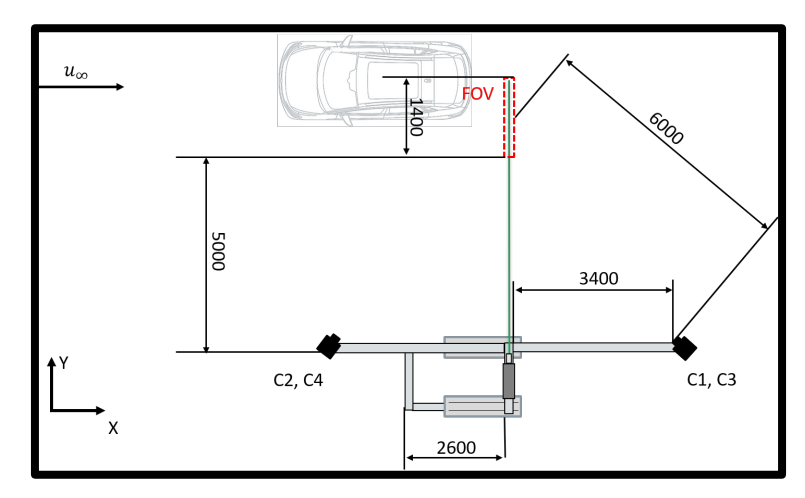


**Figure 2.** Top view of the measurement setup with the working distance annotations. All measures are given in mm.

The complete setup was prepared and initially aligned outside of the wind tunnel, in order to save time during the implementation step. Including the ground platform, the setup was placed on rollers and transferred into the wind tunnel. Adjustable feet were used to make height adjustments to the base platform. Fine adjustments on the laser light sheet were made with reference to both the wind tunnel and the designated vehicle coordinate system, ensuring the accurate positioning of the light sheet and linear movement components. High particle image signal to noise ratio was ensured by employing a pneumatic nozzle seeder with a mean output particle diameter of ~2 µm, which allows to enhance the light scattering properties of the particles (Fukuchi, Sawada, Nakajima, & Murakumo, 2016). The particle size was approximately 3 px and the seeding density was between 0.05 - 0.07 ppp.

Component	Amount	Company Type		
Camera	4x	LaVision	Imager SCMOS CLHS 5 MP	
Lens	4x	Zeiss	M. Planar Interlock f = 100 mm f# = 2.0	
Timing Unit	1x	LaVision	Programmable Timing Unit (PTU)	
Laser	2x	Lumibird Quantel	Evergreen 200	
Seeding generator	1x	Seika Digital	CTS Quad	
		Imaging/ILA 5150		
Seeding Medium	-	-	DEHS	
Linear Movement Unit	2x	Isel	Heavy duty traverse - 1500 mm	
Mounting	-	Qioptiq	X95	
Calibration Plate	1x	Volkswagen	Custom built 3D 1400x1400x60 mm <sup>3</sup>	
Software	_	LaVision	DaVis 10.2.1	

**Table 1.** Experimental apparatus

The geometrical calibration was done using a two-sided 3D calibration plate, which was built inhouse at Volkswagen and adopted from a previous experiment (Hüttig, Gericke, Sciacchitano, & Akkermans, 2023). A pinhole calibration model was employed. For every measurement point, a total of 4500 double frame images were acquired with a rate of 16 Hz. A total of 82 measurement points on 9 traversed positions were captured. A time separation of  $\Delta t = 60 \, \mu s$  between laser pulses was used. The resulting maximum particle between frames was measured to be 7 px. From the 9 traversed positions, only 3 planes are shown in this study. These planes are displayed in Figure 4, positioned within the vehicle coordinate system. P1 is positioned 1 m in the wake, P2 0.3 m and P3 is positioned directly behind the vehicle. Two ride heights have been comparatively investigated. One being the standard configuration with a 798/795 mm (front/rear) ride height and the lower ride height configuration with a 784/781 mm (front/rear). Both height measurements correspond to the distance between the wind tunnel floor and highest point of the wheel housing. The free stream velocity during the measurements was set to 38.89 m/s. In addition to the PIV measurements, the wind tunnel force balance measurements were recorded, so that an association between the flow topology and the aerodynamic drag coefficient could be made.

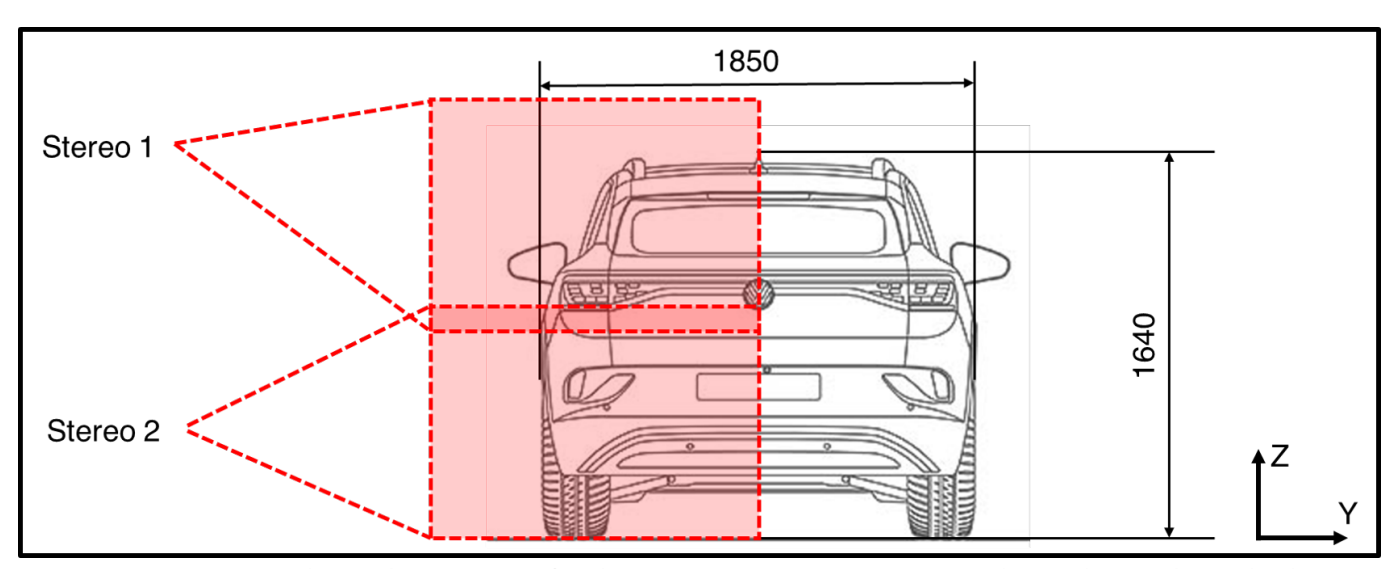
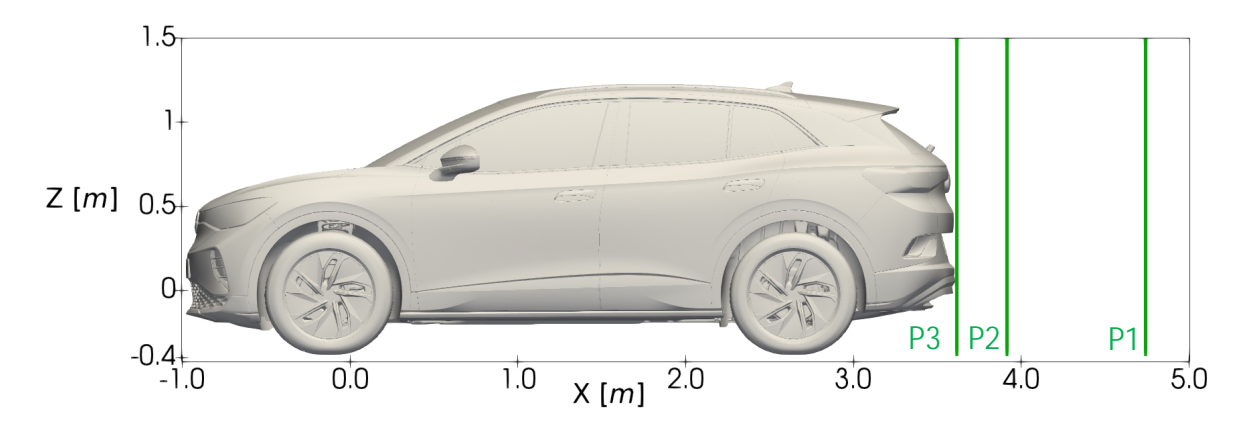


Figure 3. Example of the FOVs of both stereo camera systems in the wake of the vehicle.

The acquired particle images were processed using the latest DaVis 10.2.1 software. The two stereo PIV systems were processed separately, and the instantaneous velocity vector fields of both areas were then stitched together. A multi pass cross-correlation evaluation was performed on the images which started with a 128 x 128 px² interrogation window and ended after 4 passes at 64 x 64 px² with 75% overlap. The cameras had a magnification factor of 2.33 px/mm and thereby the resulting grid spacing was 6.866 mm. The geometrical calibration could not be performed on every measured plane position. The calibration was performed in the wake of the vehicle and the

misalignments of the geometrical calibration and the laser light sheet plane were corrected using the Disparity Correction or Self Calibration function of DaVis. Additionally, the slight misalignments caused by the traversing movements have been corrected using the same function (B. Wieneke, 2005). Lastly, the achieved 3C velocity vector fields were exported to the open-source visualization software ParaView for further analysis.



**Figure 4.** PIV Planes displayed within the vehicle coordinate system.

#### 3. Results

The average velocity vector fields were generated using 4500 instantaneous velocity fields for each measurement point. This study was primarily undertaken to validate the Computational Fluid Dynamics (CFD) models utilized by the aerodynamic development team at Volkswagen AG. Consequently, particular emphasis was placed on the averaged velocity fields, given their significance in this validation process. The high number of images used per measurement point was required to ensure sufficient convergence and reduce the uncertainty of the predominant velocity component, which was in the the out-of-plane direction. Depending on the local light sheet thickness and the occurrence of lost particle image pairs between frames, the statistical convergence of the average velocity fields is reached slowly. A substantial amount of independent measurement instances ensured better statistical convergence. The assessment of convergence was conducted by establishing a confidence interval based on the last 200 averaged velocity vectors from a pool of 4500 values at three designated points, see Figure 5. For point 'a', the average u-velocity value was determined to be 38.4363 ± 0.0009 m/s with a confidence level of 99.7%. Similarly, for point 'b', the corresponding value was 21.9877 ± 0.0043 m/s, and for point 'c', it was 2.8612 ± 0.0086 m/s, both with a confidence level of 99.7%. The convergence plots of these corresponding points are also a good way to evaluate the convergence of the average velocity, see Figure 6. The convergence plots show that 4500 3C velocity vector fields were necessary to achieve convergence in the shear layer and the wake.

Another way of assessing the capabilities of the present measurement is calculating the dynamic spatial- and velocity ranges (Adrian, 1997), (Scharnowski & Kähler, 2020). The dynamic spatial range DSR is defined by the camera sensor resolution and the final interrogation window size, which can be calculated by:

$$DSR = \frac{X_{max}}{D_I} = \frac{2560 \, px}{64 \, px} = 40 \tag{1}$$

The dynamic velocity range (DVR) can be defined by the ratio of the highest measurable velocity to the lowest resolvable velocity by the measurement system:

$$DVR = \frac{\Delta X_{max}}{\sigma_{\Delta x}} = \frac{U_{max}}{\sigma_{U}} \tag{2}$$

In measurements, where the main component of the flow is the out of plane component, the upper limit of the velocity range is defined by experimental boundaries such as the light sheet thickness. The lowest resolvable velocity can be defined as the (local) uncertainty of the instantaneous velocity estimation of the given measurement system. According to Wieneke (Bernhard Wieneke, 2015), the uncertainty in PIV lies generally at about 0.1 px and looking at the present data, this corresponds to 0.7 m/s. The maximum resolvable velocity is limited by the light sheet thickness since the main flow component is the out of plane motion. Therefore, the light sheet thickness is taken as a theoretical limit of a particle movement between pulses to be captured. This corresponds to 133 m/s and thereby:

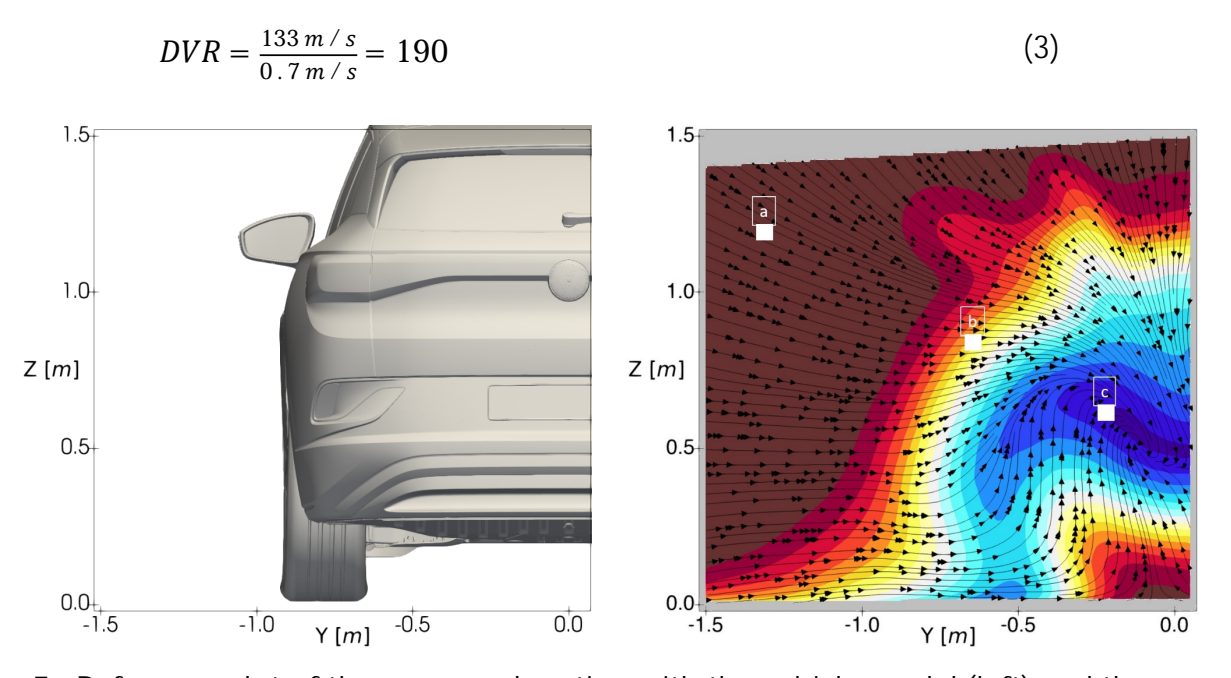


**Figure 5.** Reference plot of the measured section with the vehicle model (left) and the averaged velocity vector field at plane P1 with normal ride height (right)

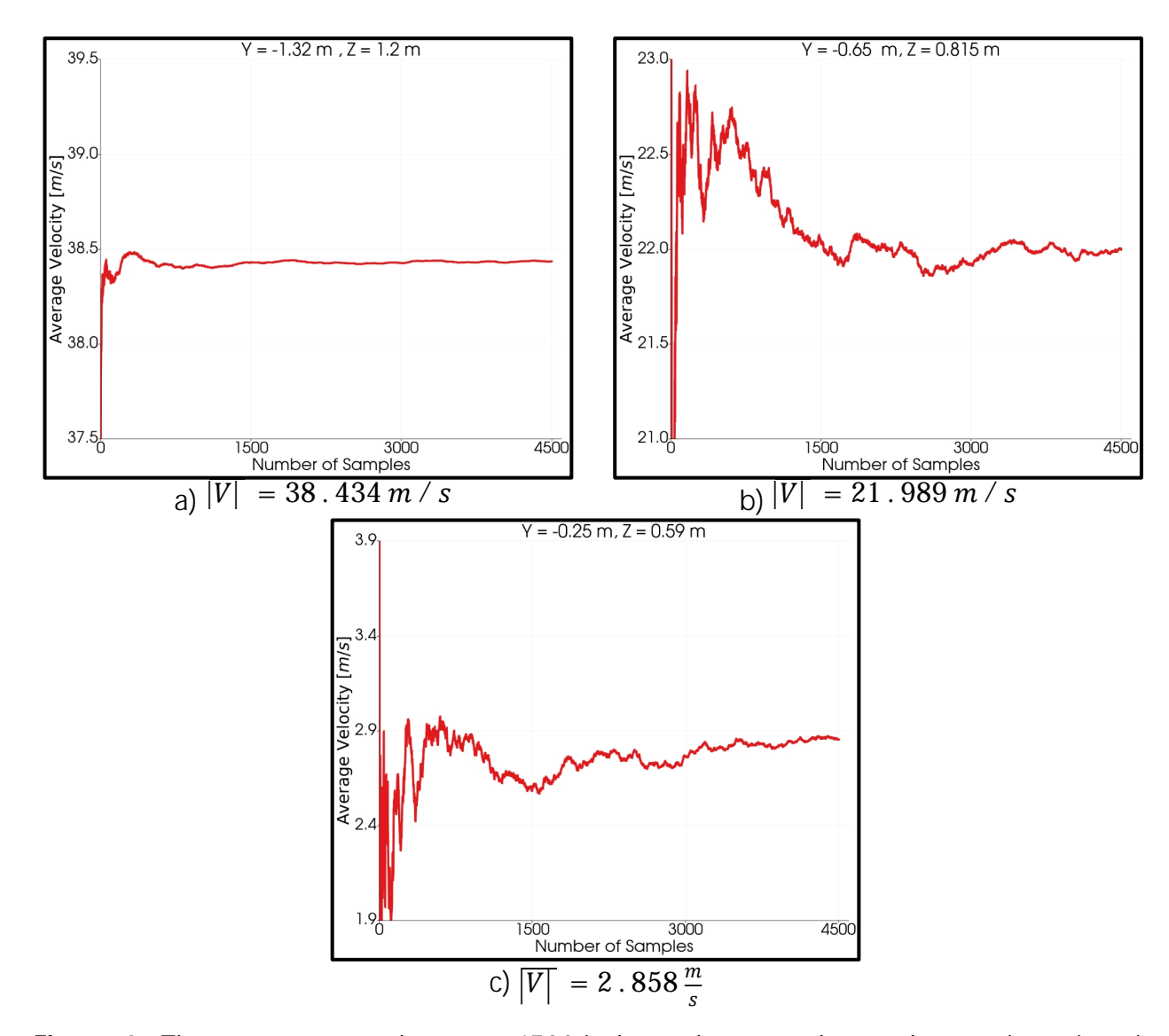


**Figure 6.** The convergence plots over 4500 independent samples on three points given in Figure 5 in free stream (a), shear layer (b) and wake (c) positions in the measurement area.

The wind tunnel balance measurements pose a good initial information source on the global effects of ride height changes, The data can be associated with the flow topology measured by PIV. On Table 2 the drag and lift coefficients relative to the median of the values of all measured vehicle configurations are given. Looking at the  $\mathcal{C}_d$  values it can be said that the reduction of the ride height caused a reduction in the overall drag coefficient of the vehicle.

The average velocity fields of both ride heights measured on P1, P2 and P3 are displayed comparatively on Figure 7. The velocity fields depicted in Figure 7a and 8b show to have differences in the flow around the taillights, as framed within the red boxes. On the measured plane of P2 (Figure 7b and 8c), which corresponds to the plane measured 0.3 m away from the vehicle, the differences become more significant, and the trailing vortices are present in different forms. The flow in the separation bubble of both configurations show two counter rotating recirculation regions pulling the air from the ground up, where the normal ride height displays equally sized vortices (Figure 7c). The low ride height yields one relatively larger vortex on the middle left of the

recirculation region and the smaller on the bottom close to the symmetry line of the vehicle (Figure 7d). In accordance with the presented velocity fields on Figure 7, two distinct wake topologies emerge depending on the configuration. The measured configuration demonstrates the occurrence of both these types of wake topologies across varying ride heights, as depicted in Figure 7e and 7f. Under normal ride height conditions, the vehicle exhibits a broader but lower wake region, with a downwash observed between Z = 0.5 m - 1.4 m around the symmetry axis of the vehicle. This configuration aligns with the wake structure of a generic fastback vehicle model previously characterized by Ahmed (1981). The examination of the low ride height measurement on the other hand reveals a narrower wake and recirculation region, predominantly filled by airflow from the sides, which in this case corresponds to the topology of an estate-back vehicle, as presented by Ahmed (1981) and Avadiar et al. (2018).

An additional tool to characterize the turbulence in the shear layers and of the vehicle, is the turbulent kinetic energy (TKE), which is extracted from the fluctuation velocity vectors of the PIV data. The displayed TKE fields of the P1 plane on Figure 8 also confirms the differences in flow topology identified within two types of wake topology using the velocity fields. Within the normal ride height configuration, the flow tends to be more turbulent in the underbody region, while the low ride height configuration results in a higher turbulent region on the top of the wake region (both displayed in red frames on Figure 8).

According to Varney et al. (2020) the rear flow of an estate back vehicle poses significant differences from those of notch and fastback geometries. This statement is based on pressure tap measurements, wind tunnel balance measurements and PIV measurements on all three rear geometries of the DrivAer model. The connection between the wake flow topology and the drag /lift coefficients was also presented within the study of Ahmed (1981).

A value which can be associated with the flow topology, is the significant difference in the rear lift of both configurations. The normal ride height configuration with the fast back type wake topology shows to have a significant difference to the rear lift of the low ride height configuration with the estate back type flow topology. The rear lift coefficient shows to decrease with a significant 0.045, when the configuration is shifted from normal ride height to low ride height.

Configuration	$\Delta C_d$	$\Delta C_{lf}$	$\Delta C_{lr}$
Normal Ride Height	0.003	0.002	0.0195
Low Ride Height	-0.006	-0.003	-0.0255

**Table 2.** Drag and lift coefficient values of both ride heights. The values given do not correspond to the absolute measured values and are given as a difference to the median value from all the measured configurations.

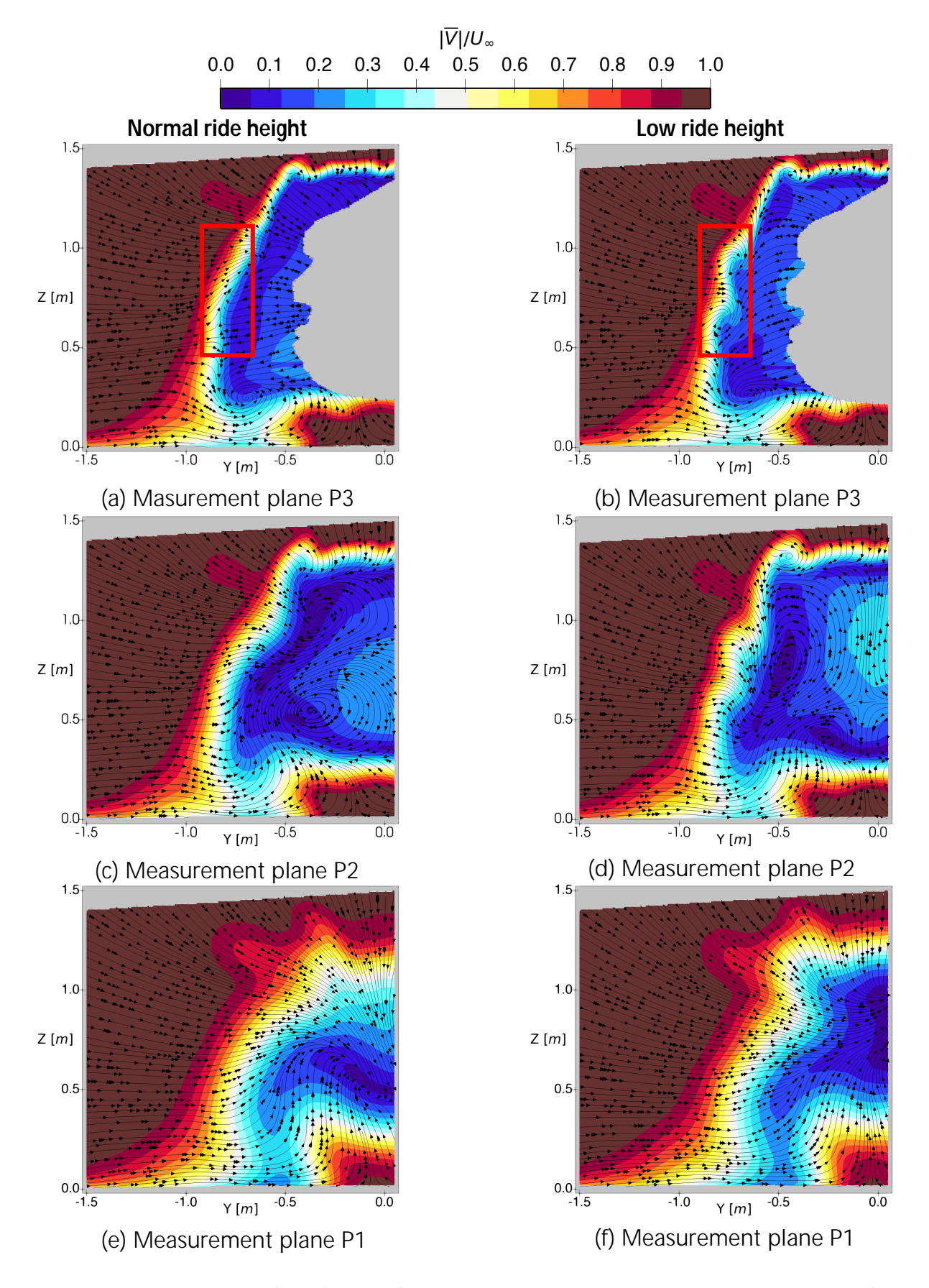


**Figure 7.** Velocity vector fields of both ride height configurations on the three measured planes.

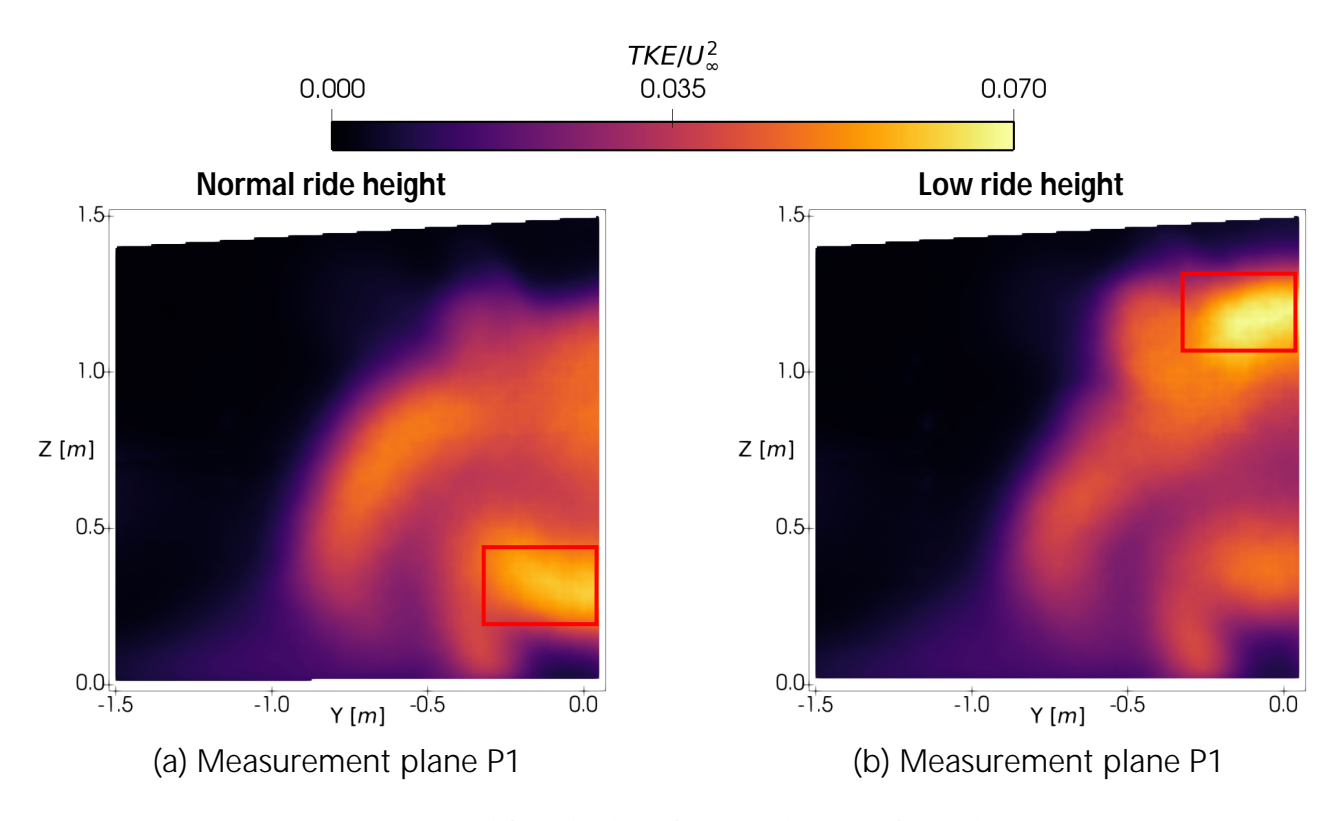


**Figure 8.** TKE fields calculated using the PIV data plane 1.

#### 4. Conclusions

The near wake of a Volkswagen ID.4 was characterized by analyzing PIV data in the near wake of the vehicle and the wind tunnel balance measurements. A change of ride height variation of 14 mm has shown to have global effects on the wake topology of the ID.4. The vortical structures and the dissipation characteristics of vortices of both ride height configurations show strongly similar values of topologies from different rear shaped vehicles within previous research (Ahmed, 1981; Hucho, 2013; Varney et al., 2020). The normal ride height variation showed to yield a wake form typical of a fast back or a notch back vehicle. Lowering the ride height variation by 14 mm caused the wake topology to shift towards the form of a typical estate back type vehicle. The shift to low ride height has also shown to cause a reduction of 0.009 in  $C_D$ , 0.005 in  $C_{If}$  and 0.045 in  $C_{Ir}$ . The reduction of the drag coefficient by 0.009 can be associated with the reduction of the ride height, which complies with previous research (Francesco Fabio Semeraro, 2022). However, the present study shows that this connection cannot be made with the near wake flow topology of both types. Just by looking at the change in wake topology and previous research by Ahmed and Varney, the expectation would be that the  $C_D$  value would increase as the reduction in ride height shifts the wake topology to that of an estate back vehicle. In the contrary to the studies made with various

rear forms, no significant change on the vehicle rear was made within the present experimental study. Therefore, it is difficult to make a statement about the cause of this, just by looking at the near wake of the vehicle. Further experiments closer to the rear wheels and in the underbody of the vehicle are necessary to understand how such global changes are caused in the wake of the vehicle and how they effect the aerodynamic drag coefficient. An understanding of the flow interactions of tire deformations caused by the ride height changes are required to generate a better understanding of global effects. The front lift values show also to be relatively unaffected by the ride height changes. On the other hand, the topology differences caused by ride height reduction comply with the expected effects on the rear lift coefficient. This indicates that the downwash from the normal ride height with the fast back type topology might have caused a higher rear lift value.

In summary, the measurement concept has demonstrated promising outcomes in terms of both applicability within a short time frame and quantity of recorded data at a satisfactory quality. The utilization of a seeding generator producing particles with a mean diameter of ~2 µm allowed large -scale PIV experiments using Di-Ethyl-Hexyl-Sebacate (DEHS), enabling the investigation of global aerodynamic effects from subtle design changes or different vehicle configurations. Technological advancements and integrated software and hardware have made such experiments increasingly viable for relatively small-scale projects like passenger car aerodynamics R&D. The adoption of similar setups with higher resolution cameras, readily available in the current market, also presents the opportunity to evaluate the turbulence intensity of industrial wind tunnel facilities in future studies.

The results, opinions and conclusions expressed in this publication are not necessarily those of the Volkswagen Aktiengesellschaft.

## **Acknowledgments**

The author would like to acknowledge the support of the aerodynamics and laser metrology teams of Volkswagen AG. In addition, the author would like to deeply acknowledge the support of the team of AS-EXV from the German Aerospace Center for their extraordinary support during the measurement campaign.

#### References

- Adrian, R. J. (1997). Dynamic ranges of velocity and spatial resolution of particle image velocimetry. Measurement Science and Technology, 8(12), 1393–1398. doi:10.1088/0957-0233/8/12/003
- Ahmed, S. R. (1981). Wake Structure of Typical Automobile Shapes. Journal of Fluids Engineering, 103(1), 162–169. doi:10.1115/1.3240767
- Avadiar, T., Thompson, M. C., Sheridan, J., & Burton, D. (2018). Characterisation of the wake of the DrivAer estate vehicle. Journal of Wind Engineering and Industrial Aerodynamics, 177, 242–259. doi:10.1016/j.jweia.2018.04.013
- Francesco Fabio Semeraro, P. S. (2022). Numerical Investigation of the Influence of Tire

  Deformationand Vehicle Ride Height on the Aerodynamics of Passenger Cars. Fluids, 7(2),

  47. doi:https://doi.org/10.3390/fluids7020047
- Fukuchi, Y., Sawada, J., Nakajima, M., & Murakumo, Y. (2016). Development of a New Pressure

  Measurement Technique and PIV to Validate CFD for the Aerodynamics of Full-scale

  Vehicles. SAE International Journal of Passenger Cars Mechanical Systems, 9(2), 808–816.

  doi:10.4271/2016-01-1623
- Hucho. (2013). Aerodynamik des Automobils. (T. Schütz, Ed.)Aerodynamik des Automobils. Springer Fachmedien Wiesbaden. doi:10.1007/978-3-8348-2316-8
- Hüttig, S., Gericke, T., Sciacchitano, A., & Akkermans, R. A. D. (2023). Automotive on-road flow quantification with a large scale Stereo-PIV setup. 15th International Symposium on Particle Image Velocimetry ISPIV 2023.

  doi:http://hdl.handle.net/20.500.12680/5h73q343c
- Petar Georgiev, P. G. Giovanni De Filippis, & Sorniotti, A. (2023). On the Benefits of Active Aerodynamics on Energy Recuperation in Hybrid and Fully Electric Vehicles. Energies, 16(15), 5843. doi:10.3390/en16155843

- Scharnowski, S., & Kähler, C. J. (2020). Particle image velocimetry Classical operating rules from today's perspective. Optics and Lasers in Engineering, 135, 106185.

  doi:10.1016/j.optlaseng.2020.106185
- Varney, M., Passmore, M., Wittmeier, F., & Kuthada, T. (2020). Experimental Data for the Validation of Numerical Methods: DrivAer Model. Fluids, 5(4), 236. doi:10.3390/fluids5040236
- Wieneke, B. (2005). Stereo-PIV using self-calibration on particle images. Experiments in Fluids, 39(2), 267–280. doi:10.1007/s00348-005-0962-z
- Wieneke, B. (2015). PIV uncertainty quantification from correlation statistics. Measurement Science and Technology, 26(7), 074002. doi:10.1088/0957-0233/26/7/074002